Double-Shell-Target Implosion by Four Beams from the GEKKO IV Laser System

Y. Kitagawa, N. Miyanaga, H. Hama, T. Yabe, K. Fujiwara, Y. Kawai, M. Nakatsuka, T. Norimatsu, Y. Izawa, T. Yamanaka, and C. Yamanaka
Institute of Laser Engineering, Osaka University, Suita, Osaka 565, Japan

(Received 10 June 1981; revised manuscript received 19 April 1983)

A double-shell-target implosion was studied with the GEKKO IV glass-laser system. The inner-shell trajectory, recorded for the first time by a newly developed two-frame x-ray shadowgraphy technique, was analyzed by a self-similar flow model, implying more than 20% outer-inner kinetic-energy conversion. The trajectory also agreed with a one-dimensional code result including a vacuum insulation effect. A two-dimensional particle-in-cell simulation analyzed the illumination nonuniformity printed on the inner shell.

PACS numbers: 52.50.Jm, 52.55.-s, 52.70.-m

Double-shell targets for laser and beam fusion are very interesting,[1-7] because they are expected to have many advantages over single-shell designs. A massive outer shell multiplies the inner-shell implosion velocity and an intermediate vacuum layer makes the inner shell insensitive to hot-electron preheat, leading to cold and therefore more efficient compression. Nevertheless, few experimental studies are known. We present here results for a double-shell-target implosion using four beams from the GEKKO IV 1.053-μm laser system. A newly developed two-frame x-ray shadowgraphy technique enabled us to record the inner-shell trajectory and deformation for the first time. The trajectory was compared with a one-dimensional (1D) Lagrangian simulation and also analyzed with a self-similar flow model, which implied that more than 20% of the outer-shell inward kinetic energy was converted to that of the inner shell. To investigate double-shell target uniformity, we compared shell deformations with a 2D particle-in-cell (PIC) simulation.

A microscopic photograph of the target is shown in Fig. 1(a) and its schematic cross section in Fig. 1(b). A pair of 2-μm-diam glass fibers fixed the inner shell, containing 0.2-atm residual nitrogen, at the outer-shell center. Four lenses ($f/1.5$) focused tetrahedrally symmetric beams [total of (90 J)/(200 ps) on target, 4.4×10^{14} W/cm^2] tangentially to the target, as shown in Fig. 1(c).[8]

Two-frame x-ray shadowgraphy, shown in Fig. 2, provided sequential pinhole images by one shot.[9] Probe beam 1 and probe beam 2 [(15 J)/(200 ps) each and 300-ps separation], focused on a molybdenum plane target, produce two 200-μm-diam plasmas sequentially, emitting sequential pulses of 2.6-keV–centered x rays, which are selectively absorbed by the inner-shell sili-

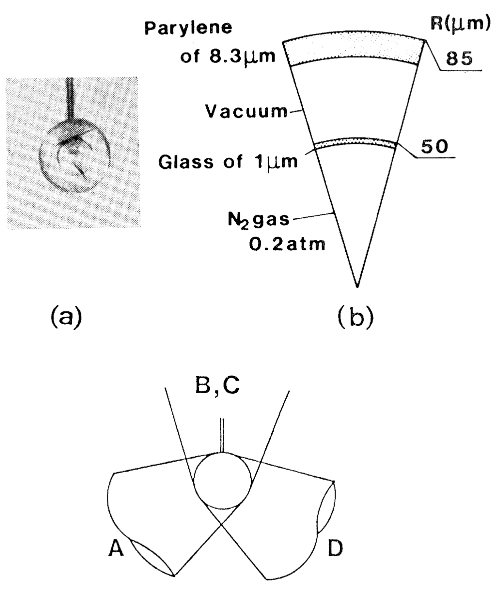

FIG. 1. (a) Microscopic photograph of double-shell target. (a) Schematic cross section of double shell. (c) Tangential illumination of A, B, C, and D laser beams.

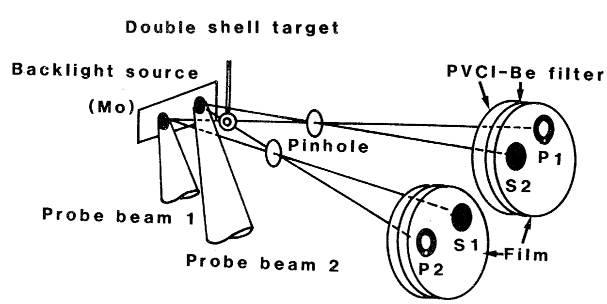

FIG. 2. Two-frame x-ray shadowgraphy. Probe beam 1 precedes probe beam 2 by 300 psec. Source image $S1$ and target image $P1$ are from probe beam 1; $S2$ and $P2$ are from probe beam 2.

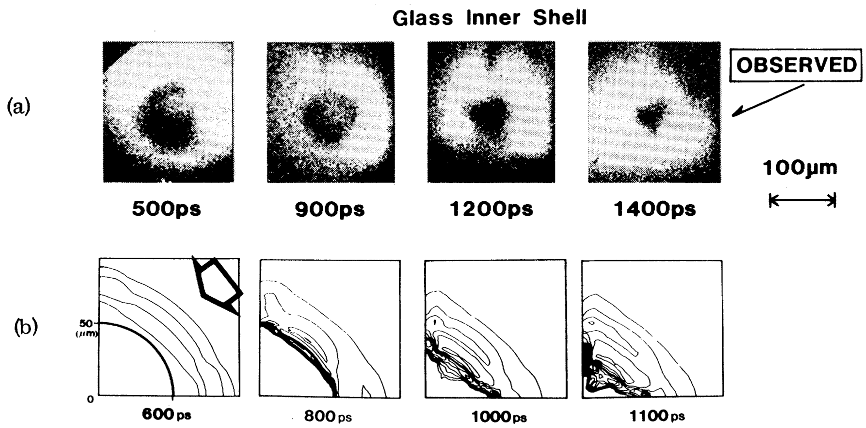

FIG. 3. (a) Inner-shell x-ray shadow images. (b) Double-shell density contours by 2D PIC code IZANAMI in 0.2-g/cm^3 increments. The arrow shows the incident beam.

con K edge. X rays from probe beam 1 (or 2) produce both a source image $S1$ (or $S2$) and a source image through the shell $P1$ (or $P2$) on Kodak no-screen films. A tantalum pinhole is 22 μm in size and a filter is made of 22-μm-thick polyvinyl chloride and 55-μm-thick beryllium.

Figure 3(a) shows inner-shell shadow images at various delay times after the main laser pulse. The shell diameter begins to decrease between 0.5 and 0.9 ns and triangular shell deformations appear at 1.2 and 1.4 ns, which are strongest along the laser-illumination directions. Figure 3(b) shows the double-shell density contours simulated by the 2D PIC code IZANAMI,[10] where the laser is focused axisymmetrically 45° from the vertical axis, as shown by an arrow. Another pellet-target experiment at 10^{14} W/cm^2 determined 6% resonance and 6% inverse-bremsstrahlung absorptions.[11] A one-group flux-limited diffusion model estimated the hot-electron transport. Contours in the figure are in 0.2 g/cm^3 increments.

On the other hand, the 1D Lagrangian code HIMICO simulated the implosion dynamics shown in Fig. 4.[12] For 4.4×10^{14} W/cm^2 and 5% resonance absorption, the code yields 7.5% inverse-bremsstrahlung absorption and 0.6% radiation loss. A multigroup flux-limited diffusion model estimated the hot-electron transport. Since we assume a flux limit of $f=0.03$, the cold-electron temperature becomes 1.5 keV at the critical density. The Estabrook and Kruer formula[13] estimates the hot-electron temperature to be 7 keV, yielding a 9-μm energy deposition range comparable with the shell thickness and a 37-Mbar preheat pressure driving the outer shell explosively rather than ablatively.[14] So, although we have no clear, direct experimental confirmation, we suppose that the hot electrons heat and explode the outer shell, but not the inner shell because of the vacuum layer. Saha's equation models the ionization stages.

Because experimental shell images were tri-

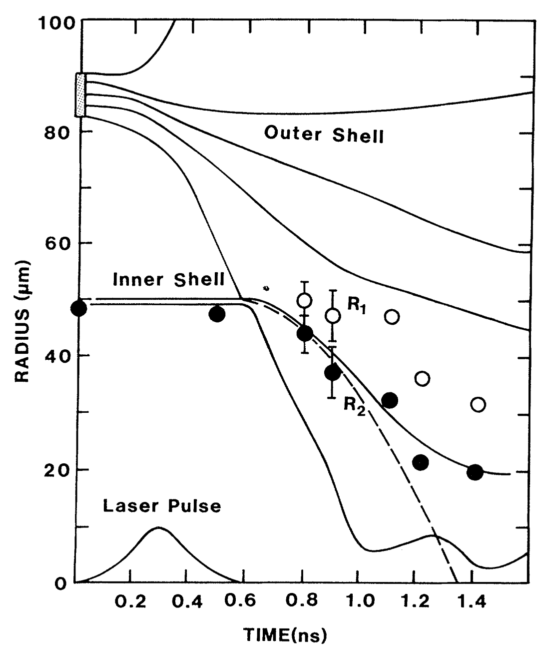

FIG. 4. The maximum radius R_1 (open circles) and minimum radius R_2 (solid circles) of the inner glass shell vs time. The lines are the outer- and inner-shell radii simulated by the 1D Lagrangian code HIMICO. The dashed line is the inner-shell trajectory R after the self-similar flow model.

TABLE I. Comparisons of the inward kinetic energy E_{kin}, the imploding velocity, and the hydrodynamic efficiency η_H between model and experiment. 12% of 90 J incident is absorbed.

Time (ns)	Outer shell E_{kin} (J)	Outer shell η_H (%)	Conversion (%)	Inner shell E_{kin} (J)	Inner shell η_H (%)	Experiment E_{kin} (J)	Experiment η_H (%)
1.0	0.58	5.3	34	0.20 (7.2×10^6 cm/s)	1.8	0.12 (5.4×10^6 cm/s)	1.1
1.2	0.6	5.5	58	0.35 (9.4×10^6 cm/s)	3.2	Stagnate	

angularly deformed, in Fig. 4 we have plotted R_1 (the radius of the circle circumscribed to the image) and R_2 (that inscribed to the image) as the maximum and minimum locations of the outer-inner shell contact surface; vertical error bars indicate several-shot reproducibility. The 200-ps pulse and 22-μm pinhole limited the temporal and spatial resolutions. The mean contact surface velocity $\bar{u}$ is 5.4×10^6 cm/s.

We can treat the outer-shell motion by a self-similar flow model, if hot-electron preheat expands the outer shell around its mass center, which pushes the solid inner shell. If both hot-electron and shock preheats are neglected as well as spherical effects, the inner-shell motion is

$$(\rho r)_{in}\, d^2X/dt^2 = P(X,t),$$

where $(\rho r)_{in}$ is the inner shell ρr and X is its location. The pressure $P(X,t)$ is given from self-similar solutions of the outer-shell flow as[15]

$$P(X,t) = 0.55\, C_s^{\,2}\rho(X,t) + v^2\rho(X,t),$$

where

$$\rho(X,t) = \rho_0 \frac{\xi(0)}{\xi(t)} \exp\left[-\left(\frac{X}{\xi(t)}\right)^2\right],$$

$$v(X,t) = \dot{\xi}(t)X/\xi(t),$$

$$\xi(t) \simeq 1.1\, C_s(t - 8\times10^{-11}),$$

and ρ_0 and C_s are the initial outer-shell density and sound velocity, respectively, t is in seconds, and $X = R_0 - R$. R is plotted in Fig. 4 by the dashed line. The model agrees with the 1D HIMICO result until 1.2 ns, when 11 J is absorbed from 90 J on target and 5.5% of the absorbed energy is transferred to the outer-shell inward kinetic energy ($E_{kin} = 0.6$ J, hydrodynamic efficiency $\eta_H = 5.5\%$), 58% of which is then converted to the inner-shell kinetic energy ($E_{kin} = 0.35$ J, $\eta_H = 3.2\%$), yielding 0.4% overall energy efficiency of the target. Comparisons of E_{kin}, the imploding velocity, and η_H between model and experiment at 1 and 1.2 ns are listed in Table I, and imply that in the experiment more than 20% of the outer-shell inward kinetic energy is converted to that of the inner shell ($\eta_H > 1.2\%$, overall $> 0.13\%$) and that hot-electron preheat is not dominant for the shell compression. After 1.2 ns, the experimental points stagnate as a result of a spherical effect or a reflected shock wave, because the shock wave of velocity $2\bar{u}$ ($= 1.1\times10^7$ cm/s) reflects at the center and reaches the contact surface again at 1.2 ns. Since the model estimates the mean inward velocity of the outer shell as

$$\langle v\rangle = (2/M)\int_0^\infty \rho_0 v\, dx = 4.9\times10^6 \text{ cm/s},$$

where M is the shell mass, the inner shell is scarcely velocity multiplied (~1.1). The shock theory implies that the shell preheat temperature is as low as 80 eV.

At 1.4 ns (time of maximum compression), R_2 becomes 20 μm, the pinhole resolution limit, which gives an estimate of the inner-shell $\rho\Delta R$ as 3.2×10^{-3} g/cm^2 close to the simulated 5.3×10^{-3} g/cm^2. To describe the R_1 implosion delay relative to that of R_2, we used the 2D code IZANAMI and analyzed the shell deformation amplitude $(R_1 - R_2)/R_0$ as a function of time, shown in Fig. 5, where the line is the simulation and R_0 is the initial inner-shell radius. The experimental plot becomes maximum 0.2 ns prior to the maximum compression, coincident with the simulation, which shows that R_1 is still imploding when R_2 already stagnates near the maximum compression.

In summary, newly developed x-ray framing shadowgraphy observed inner-glass-shell compression to 20 μm radius at 1.4 ns, whose trajectory was in agreement with a 1D HIMICO simulation that included vacuum insulation. The self-similar flow model, implying more than 20% outer–inner-shell kinetic energy conversion, ex-

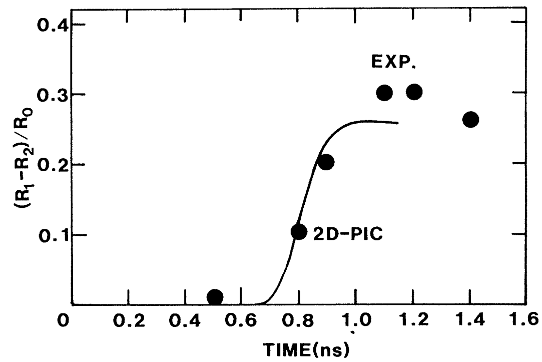

FIG. 5. Inner-shell deformation amplitude $(R_1 - R_2)/R_0$ vs time. R_0 is the initial inner-shell radius. The line is the 2D PIC IZANAMI simulation.

plains well a cold implosion of 5.4×10^6 cm/s and overall efficiency of more than 0.1%, although velocity multiplication was scarcely obtained in the present work. The 2D code IZANAMI describes the illumination nonuniformity printed on the inner shell, which shows that the deformation becomes maximum at 1.2 ns. Further study will be reported elsewhere.[16]

The authors would like to thank Dr. K. Yoshida for providing the laser system, A. Furusawa for providing double-shell targets, and Dr. K. Mima for model discussions.

[1]R. C. Kirkpatrick, C. C. Cremer, L. C. Madson, H. H. Rogers, and R. S. Cooper, Nucl. Fusion 15, 333 (1975).

[2]W. C. Mead, Laser Program Annual Report—1976, Lawrence Livermore Laboratory Report No. UCRL-50021-76, 1976 (unpublished), p. 4–39.

[3]J. D. Lindl, Laser Program Annual Report—1978, Lawrence Livermore Laboratory Report No. UCRL-50021-78, 1978 (unpublished), p. 3–10.

[4]G. McClellan, Laser Program Annual Report—1978, Lawrence Livermore Laboratory Report No. UCRL-50021-78, 1978 (unpublished), p. 3–10.

[5]P. D. Roberts, S. J. Rose, P. C. Thompson, and R. J. Wright, J. Phys. D 13, 1957 (1980).

[6]"Fusion News," Fusion 27, 68 (July 1980).

[7]B. H. Ripin, S. E. Bodner, S. H. Gold, R. H. Lehmberg, E. A. McLean, J. M. McMahon, S. P. Obenschain, J. A. Stamper, R. R. Whitlock, and F. C. Young, NRL Memorandum Report No. 4212, 1980 (unpublished).

[8]Y. Kato, Y. Mizumoto, K. Yoshida, K. Ueda, M. Monma, and C. Yamanaka, Rev. Laser Eng. 7, 35 (1979).

[9]M. H. Key, C. L. S. Lewis, H. G. Lunney, A. Moore, T. A. Hall, and R. G. Evans, Phys. Rev. Lett. 41, 1467 (1978).

[10]T. Yabe, A. Nishiguchi, and N. Ueda, Appl. Phys. Lett. 39, 222 (1981); A. Nishiguchi and T. Yabe, Institute of Laser Engineering, Osaka University, Research Report No. ILE 8132p, 1981 (unpublished).

[11]S. Sakabe and T. Mochizuki, private communication.

[12]T. Yabe, K. Mima, K. Yoshikawa, H. Takabe, and M. Hamano, Nucl. Fusion 21, 803 (1981).

[13]K. Estabrook and W. L. Kruer, Phys. Rev. Lett. 40, 42 (1978).

[14]M. H. Key, in *Laser Plasma Interactions*, Scottish Universities Summer School in Physics, St. Andrews, Scotland, 1979, edited by R. A. Cairns and J. J. Sanderson (Scottish Universities Summer School, Edinburgh, Scotland, 1980), p. 219.

[15]Y. B. Zel'dovich and Y. P. Raizer, *Physics of Shock Waves and High-Temperature Hydrodynamic Phenomena* (Academic, New York, 1966), Vol. 2, Chap. XII.

[16]Y. Kitagawa, Annual Progress Report on Laser Fusion Program, IV-2, Institute of Laser Engineering, Osaka University Report No. ILE-Apr-81, 1981 (unpublished), p. 40.

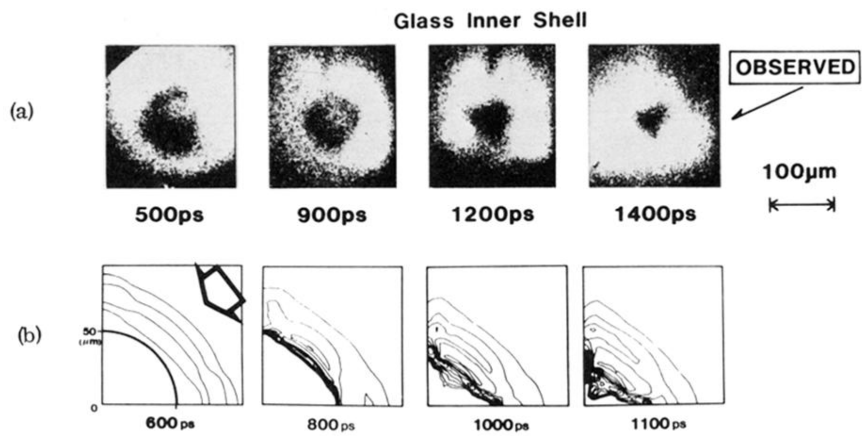

FIG. 3. (a) Inner-shell x-ray shadow images. (b) Double-shell density contours by 2D PIC code IZANAMI in 0.2-g/cm^3 increments. The arrow shows the incident beam.